Experimental and numerical study of a RC member under a close-in blast loading

Article · November 2016

DOI: 10.1016/j.engstruct.2016.08.035

Ramon Codina
National Scientific and Technical Research …

Fernanda María de Borbón
National University of Cuyo

Engineering Structures 127 (2016) 145–158

Contents lists available at ScienceDirect

Engineering Structures

journal homepage: www.elsevier.com/locate/engstruct

Experimental and numerical study of a RC member under a close-in blast loading

Ramón Codina, Daniel Ambrosini *, Fernanda de Borbón

Struct. Eng. Master Program. Eng. Faculty, University of Cuyo, Mendoza, Argentina
CONICET, National Research Council from Argentina, Argentina

ARTICLE INFO

Article history:
Received 4 February 2016
Revised 16 August 2016
Accepted 20 August 2016

Keywords:
Near field explosions
Experimental tests
Numerical simulation
RC columns

ABSTRACT

In recent years, many attacks all over the world have shown that terrorism related activity is dramatically increasing. In this context, columns are the most critical structural components and their failure is the primary cause for progressive collapse in framed structures. The effects of near-field explosions on structural elements, especially columns, have not been widely investigated in the literature. Therefore, the main objectives of this paper are: to evaluate the effectiveness of a numerical model to replicate the experimental damages of reinforced concrete (RC) columns subjected to close-in blast loading; to obtain modelling guidelines for this phenomenon and to provide quality experimental data that could be used as a reference to check the accuracy of a variety of calculation methods. For these purposes, RC members were subjected to a near field explosion in full scale. Experimental tests and numerical simulations are carried out in order to calibrate the numerical model. In this context, a new set of parameters for the constitutive equations of the concrete is proposed and verified.

1. Introduction

Blast incidents in recent years showed that most of the terrorist attacks on public structures were explosions within short standoff distance. Reinforced concrete (RC) structures are widely used in civil engineering for many reasons such as price, weathering and fire resistance but RC members have been proved to be vulnerable under explosions. In this context, columns are the most vulnerable structural components and their failure is the primary cause of progressive collapse in framed structures [1]. On the other hand, many of the research efforts in this field have been devoted to the effects of far-field explosions on structural elements. The effects of near-field explosions on structural elements, especially columns, have not been as widely investigated [2].

The current analysis methods for RC structures under blast loading consist of two major approaches, experimental and numerical studies. Bao and Li [3] studied residual strength of reinforced concrete column after blast load, and proposed a method that describes the residual strength of RC columns based on the ratio of center deflection to column height. Their research indicates that anti-seismic design of RC columns can effectively reduce the destruction of buildings under blast loading, thereby reducing the probability of progressive collapse. Parisi [4] performed a Monte Carlo simulation to obtain blast fragility surfaces and probabilistic pressure–impulse diagrams at multiple limit states which may be used for quantitative risk analysis and performance-based design/assessment. Dakhakhni et al. [5] drew Pressure–Impulse curves of RC columns and proposed a pressure – impulse bands (PIBs) technique as a tool for vulnerability screening and capacity assessment of RC column under blast loading. Zhang et al. [6] conducted an experimental study on the damage levels of RC beams under close-in blast loading, and proposed empirical equations for the deflection in the mid-span of the beams. Fujikake et al. [7] investigated the damage of RC column specimens underin blasting tests, which was required to apply blasting demolition techniques to RC buildings with rather excessive reinforcement due to earthquake resistant design. The test results revealed that the shear reinforcing bars confining the core concretes of the RC column specimens significantly affect the damage of the RC column specimens by the blasting. Also, RC members are mixed with different types of fibers and tested in order to study a possible enhancement under explosions [8,9]. Roller et al. [10] carried out a test series with columns made of normal strength concrete and advanced concrete materials subjected to contact or close-range detonation. The results demonstrate the positive influence of the different strengthening methods. Moreover, using strengthened

* Corresponding author at: Struct. Eng. Master Program. Eng. Faculty, University of Cuyo, Mendoza, Argentina.
E-mail address: dambrosini@uncu.edu.ar (D. Ambrosini).

http://dx.doi.org/10.1016/j.engstruct.2016.08.035
0141-0296/

design for a new construction results in increase of general load-carrying capacity.

Many experimental studies are not feasible because the preparations and measurements in full-scale field experiments are complex and expensive. For this reason, the experimental tests are often scaled. However, misleading conclusions may be drawn when small scale tests are extrapolated to full size specimens [8].

Numerical simulations have been widely used to better understand the influence of the blast load and the dynamic structural response in detail. The modelling of reinforced concrete (RC) members subjected to blast loads can be further complicated due to rate effects, overloading, plastic strain and spalling, among others. Many methods can be found in the literature, such as advanced single-degree-of-freedom (SDOF) model [11]; the two-step method, the model condensation method, and the new combined two-step and dynamic condensation method [12] along with complex 3D numerical models with intensive simulations, using specialized hydrocodes [13,14]. Tu and Lu [15] evaluated typical concrete models used in hydrocodes and proposed improvements of certain parameters. Yan et al. [16] reproduced numerically an experimental test [6] in order to investigate the damage mechanisms of RC beam. Li et al. [17] conducted an experimental and numerical study of reinforced ultra-high performance slabs. It is noticed that the finite element model with pre-determined material properties can reasonably reproduce the structural damage. Xu and Lu [18] studied the concrete spalling under various blast loading and structural conditions by means of a sophisticated concrete material model.

In a previous paper by the authors [19] different alternatives of protection of a RC member subjected to near field explosion were investigated. The main objectives of this paper are: to evaluate the effectiveness of a numerical model, which replicates the experimental damages of RC columns subjected to close-in blast loading; to obtain modelling guidelines for this phenomenon and to provide quality experimental data that could be used for checking the accuracy of a variety of calculation methods. For these purposes, RC members are subjected to near field explosions in full scale experimental tests and numerical simulations are carried out in order to calibrate a numerical model that can predict further results. In this context, a new set of parameters for the constitutive equations of the concrete is proposed and verified. Moreover, an erosion value for small scaled distances is recommended.

2. Preliminary studies

Prior to the experimental test, a numerical simulation was carried out in order to define the explosive location. The profiles of maximum overpressures and impulses were obtained numerically over the entire length of the column. Also, the equivalency between TNT and the commercial explosive used in the tests was verified using the results of a series of tests in free air. More details can be found in Ref. [19].

2.1. Explosive charge location

In a terrorist attack against a building, the explosive load is commonly located inside a vehicle or, alternatively, in a suitcase. In both cases, the blast load is located near the ground, generating a blast wave with higher intensity near the bottom of the column. From FEMA 426 [20], the charge of explosive than can be put inside an automobile is approximately 200 kg of TNT. A scheme of a hypothetical case is represented in Fig. 1. In order to study columns subjected to near field explosions, the vehicle is located at 3 m from the building façade, closer than the RC columns fail threshold [20]. The explosive is located 0.5 m above the ground, consistent with a car trunk.

A numerical model with an Euler mesh was built using the hydrocode AUTODYN [21]. The model had cells of 25 mm and the full model had dimensions of 4.35 m × 1.5 m × 4.0 m. The column and the ground were rigid and allowed the shock wave reflections. The air had a flow out boundary condition. The model dimensions were large enough to prevent numerical errors produced by the boundary conditions. In Fig. 2, the reflected overpressure on the column can be seen. If the ground was not present, the maximum impulse on the column would be at the same height as the center of the explosive. However, the reflections from the ground produce a wave front of the explosion that hits the column below the height at which the explosive charge is located. Profiles of maximum reflected overpressures and impulses on the column are presented in Fig. 3.

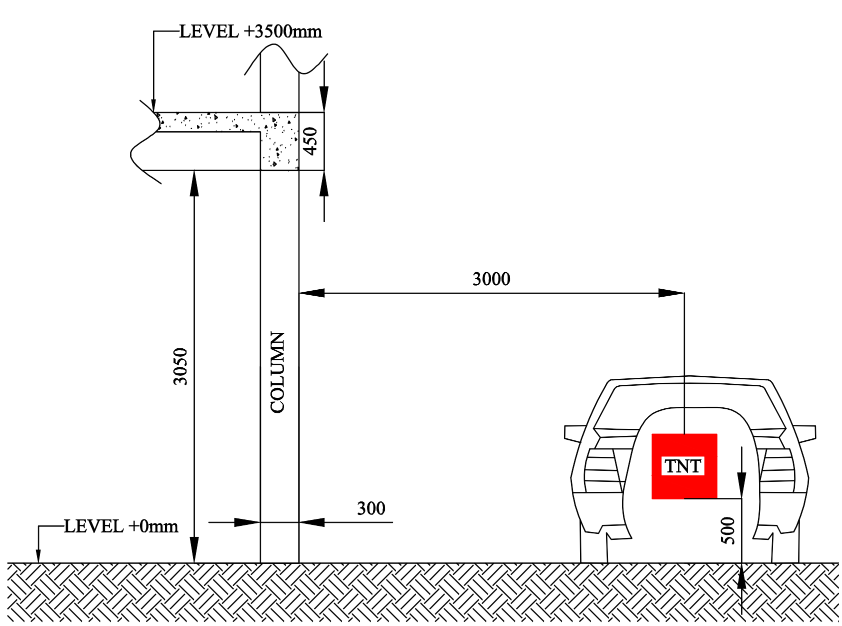

Fig. 1. Study case for profile of overpressure and impulse.

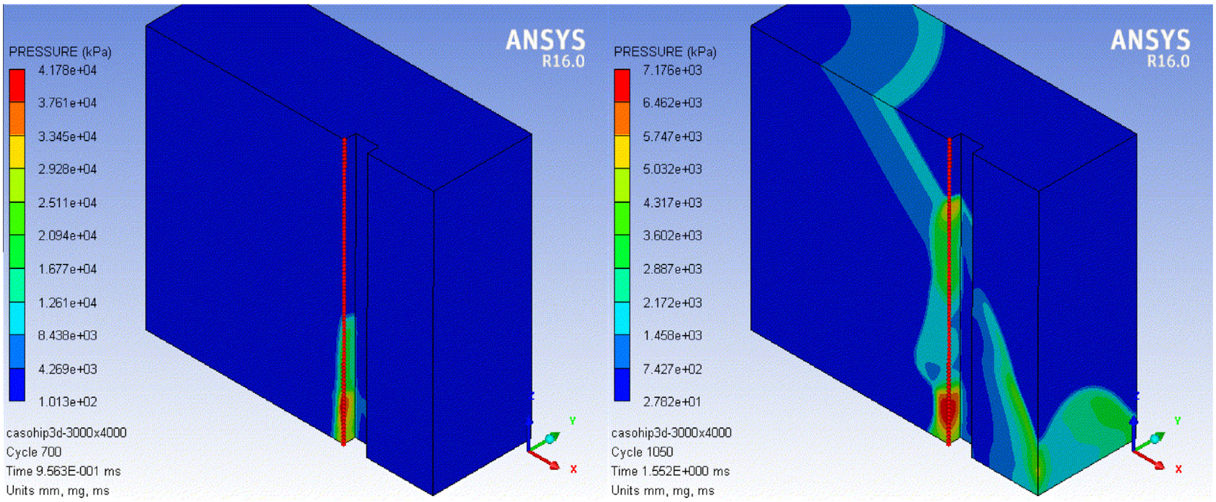

Fig. 2. Reflected overpressures for 9.56 E^{-1} ms and 1.55 ms.

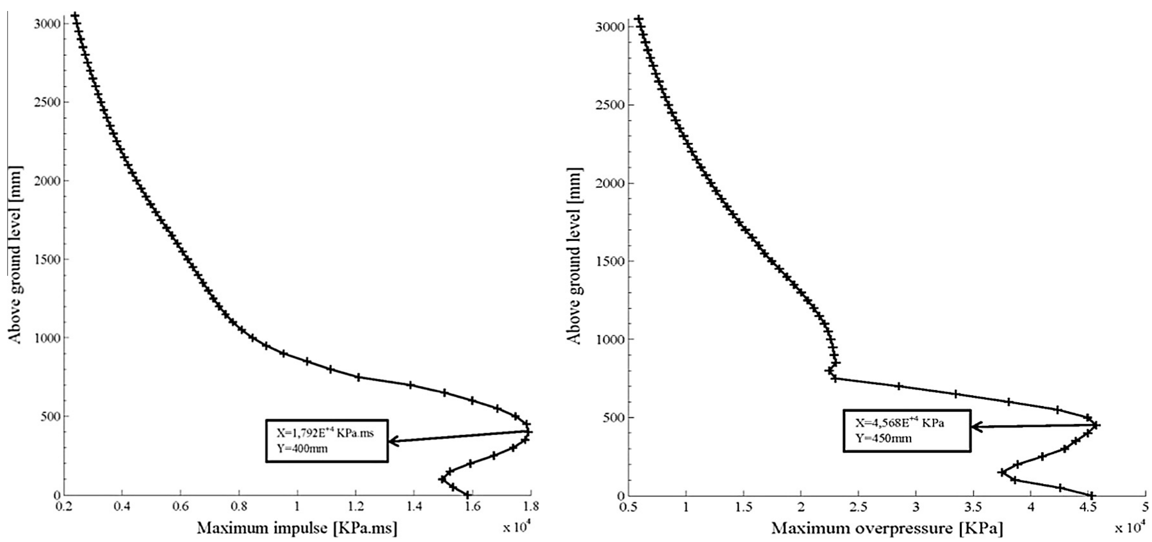

Fig. 3. Overpressures and impulses profiles.

The maximum impulse is located at 400 mm from the ground. This height represents 0.13 of the total height of the column.

3. RC member and experimental results

3.1. RC specimen characteristics

A reinforced concrete specimen was built to be subjected to blast loads. The specimen had a square section of 230 mm × 230 mm and a free span of 2.44 m. Semi–buried concrete blocks at the end of the specimen avoided the rotation of the blocks and the member. Hence, the member was assumed to be fully clamped. The concrete strength was fc = 30 MPa and the yield stress of the steel bars was f_y = 420 MPa. Transverse reinforcement was densified at the ends of the specimen within the plastic hinge region to avoid shear failure. Geometry and characteristics of the reinforcement can be seen in Fig. 4. A 20 mm clear cover was provided between the bars and the free surfaces.

3.2. Experimental setup

The specimen was tested in a horizontal position, like other studies in the literature [22]. The commercial explosive used in the tests was Gelamon VF65, a NG based gelatinous explosive theoretically equivalent in mass to 65% TNT. For the test, 8 kg of equivalent TNT was used as explosive charge. The load was cylindrically moulded and a wood framed structure was built as its support. The vertical standoff distance was measured from the center of the TNT charge to the top surface of the nude specimen and it was 100 cm (column 1) and 60 cm (column 2). Hence, the scaled distances Z were 0.5 and 0.3 m/kg$^{1/3}$, for which the tests were performed in the near field range. From the results obtained in Section 2.1, the ratio between the maximum impulse location and the column height was 0.13. Given that the member is in a horizontal position and is not influenced by the ground, the explosive was located at 0.32 m from the bottom of the member in order to obtain the maximum impulse value at 0.13 from the height of the column. The experimental set up can be seen in Fig. 5. The explosive charge was detonated using electric initiation system by a detonator which is inserted at the top of the charge.

The final deflection of the member was measured in the gauge points labelled in Fig. 5. Before the explosion, the gauge points were marked with an alcohol level, having as a point of reference an external point off the specimen that cannot be affected by the blast.

An accelerometer was located on the bottom surface of the member at 120 cm from the center of the explosive (Fig. 6). A

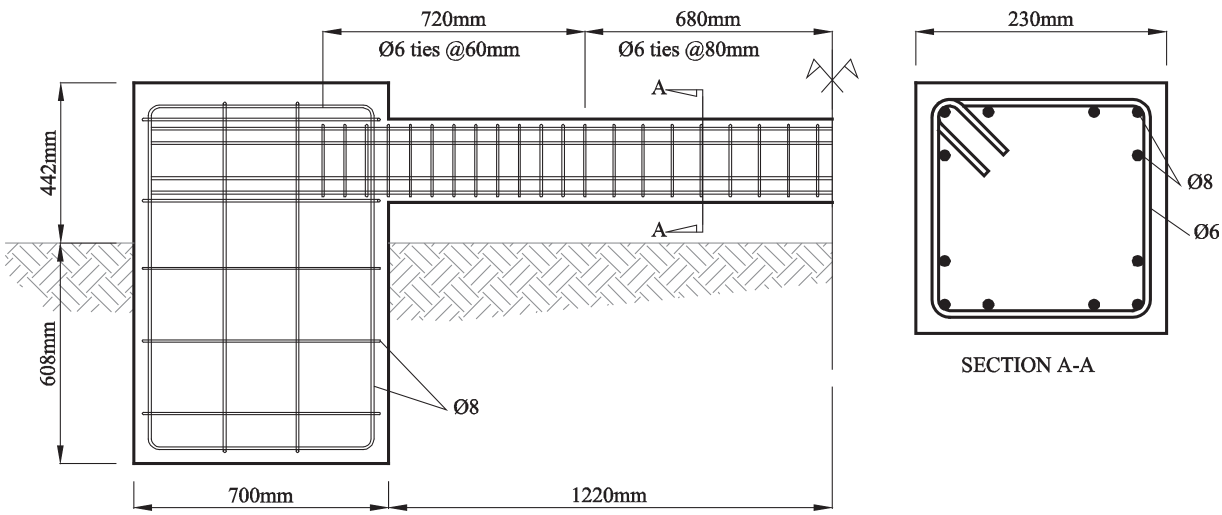

Fig. 4. Member geometry and reinforcement characteristics.

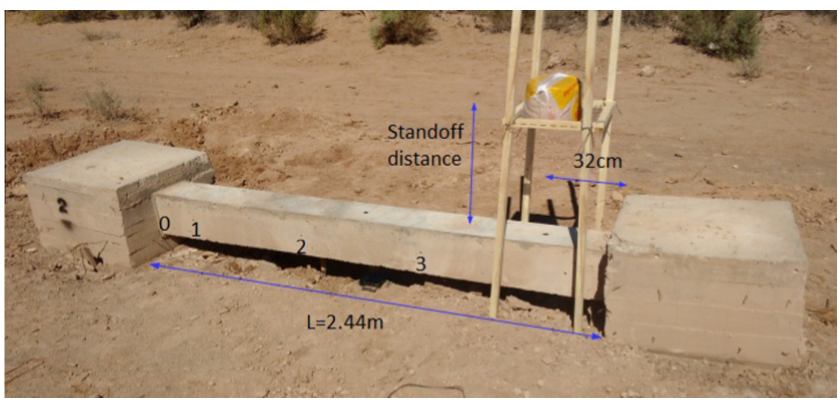

Fig. 5. Experimental setup.

Fig. 6. View of the installed accelerometer.

shock, ceramic-shear, ICP® accelerometer PCB Piezotronics model 350B21 was employed, with a sensitivity of 0.05 mV/g, a frequency range 1–10,000 Hz with a maximal error of ±1 dB and a measuring range of ±100,000 g. The accelerometer was connected to signal conditioner PCB Piezotronics 478A01. The signal was carried over a 100 m coaxial cable (RG-58) and was digitized by a data acquisition board PC-CARD-DAS16/16 using 20,000 samples per second and HP VEE 6.0 software was employed to record the time history response. All cables were duly protected using a flexible steel tube and the accelerometer was protected using a steel box (Fig. 6). The signal conditioner was buried.

3.3. Experimental results

Part of the experimental results was presented in [19]. In this section new results are given.

As mentioned in Section 3.2, two scaled distances were used in the tests. After the blast, the final gauge point positions were compared with the reference level. The measured deflections of the members are presented in Fig. 7. The final deflection, in point 3, was 84% lower for the scaled distance $Z = 0.5\ \text{m/kg}^{1/3}$ (column 1) with respect to scaled distance $Z = 0.3\ \text{m/kg}^{1/3}$ (column 2).

Both of the concrete members were damaged in flexure mode (Fig. 8) with concrete crushed on the front face, concrete spallation on the bottom surface and concrete flake off on the side surfaces. Obviously, much lesser damage was observed in column 1.

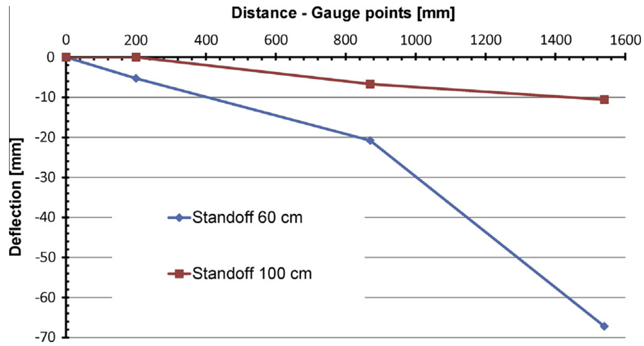

Fig. 7. Final deflection measured in gauge points.

On the other hand, time history of the accelerations measured on column 2 is showed in Fig. 9. It can be seen that the maximum measured acceleration was 11,270 g. This data is relevant in order to know the order of magnitude of accelerations in this type of problem. It should be noted that, as the accelerometer is located in an inverted position (head down), the negative accelerations should be interpreted as upwards.

4. Numerical model and results

Computer codes normally referred as "hydrocodes" encompass several different numerical techniques to solve a wide variety of non-linear problems in solid, fluid and gas dynamics. The phenomena to be studied with such programs can be characterised as highly time dependent with both geometric non-linearities (i.e., large strains and deformations) and material non-linearities (i.e., plasticity, failure, strain-hardening and softening, multiphase equations of state). In this paper, the ANSYS-AUTODYN [21] hydrocode was used through an Euler processor for the air and TNT and a Lagrange processor for the RC concrete elements. A fully coupled model with fluid-structure interaction with explicit integration is used.

4.1. Material models

4.1.1. Air

The ideal gas equation of state (EOS) was used for the air. In an ideal gas, the internal energy is a function of the temperature alone and if the gas is polytrophic the internal energy is simply proportional to temperature. It follows that the equation of state for a gas, which has uniform initial conditions, may be written as

$$p = (\gamma - 1)\rho e \tag{1}$$

in which p is the hydrostatic pressure, ρ is the density and e is the specific internal energy. γ is the adiabatic exponent defined as:

$$\gamma = 1 + \frac{R}{C_V} \tag{2}$$

where R is the universal gas constant, R_0 divided by the effective molecular weight of the particular gas and C_v is the specific heat at constant volume. Table 1 shows the properties of the air used in this study.

Where θ is the room temperature.

4.1.2. TNT

The explosive is modelled using the well known "Jones-Wilkins-Lee" (JWL) equation of state, Lee-Tarver [23]. This equation correctly reproduces the phenomenon of the expansion of gases after detonation:

$$p = A\left(1 - \frac{\omega}{R_1 v}\right)e^{-R_1 v} + B\left(1 - \frac{\omega}{R_2 v}\right)e^{-R_2 v} + \frac{\omega e}{v} \tag{3}$$

where p is the hydrostatic pressure, $v = 1/\rho$ is the specific volume, A, R_1, B, R_2 and ω (adiabatic constant) are constants and their values have been determined from dynamic experiments and are available in the literature for many common explosives. The TNT properties used in this study are shown in Table 2.

Where $V_{C\text{-}J}$, $e_{C\text{-}J}$ and $p_{C\text{-}J}$ are the C-J detonation velocity, energy and pressure respectively.

4.1.3. Concrete

An appropriate material model for concrete is critical for the reliable simulation of RC structures. For this reason, the concrete model will be described more in detail in the following. The RHT [24] model with a P-alpha [25] equation of state is used for concrete. This EOS has been proved to be capable of representing well the concrete thermodynamic behaviour at high pressures and it also allows for a reasonably detailed description of the compaction behaviour at low pressure ranges. It assumes that the initial specific internal energy for the porous material is the same as the solid material under the same pressure and temperature. The equation of state of the fully compacted or solid material is described with a polynomial function as

$$p(\rho, e) = \begin{cases} (B_0 + B_1\mu)\rho_0 e + A_1\mu + A_2\mu^2 + A_3\mu^3 & p \geqslant 0 \\ B_0\rho_0 e + T_1\mu + T_2\mu^2 & p < 0 \end{cases} \tag{4}$$

where A_i, B_i and T_i are coefficients, ρ_0 is the initial density and μ is the relative volume change.

$$\mu = \frac{\rho}{\rho_0} - 1 \tag{5}$$

The EOS for the porous material is calculated by substituting a new variable $\alpha\rho_p$ for ρ in

$$p(\rho_p, e, \alpha) = \begin{cases} (B_0 + B_1\bar{\mu})\rho_0 e + A_1\bar{\mu} + A_2\bar{\mu}^2 + A_3\bar{\mu}^3 & p \geqslant 0 \\ B_0\rho_0 e + T_1\bar{\mu} + T_2\bar{\mu}^2 & p < 0 \end{cases} \tag{6}$$

$$\bar{\mu} = \frac{\alpha\rho_p}{\rho_0} - 1 \tag{7}$$

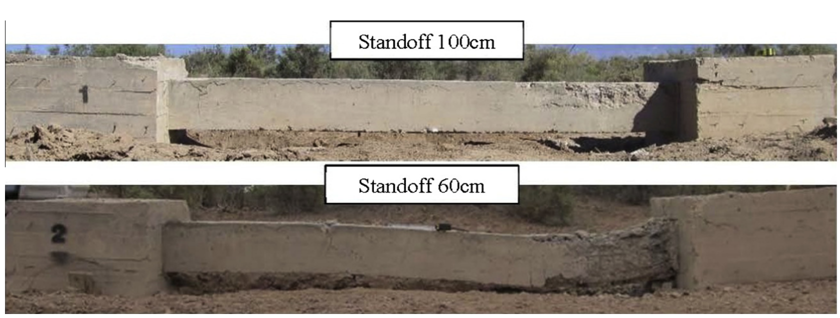

Fig. 8. Global view of the tested members.

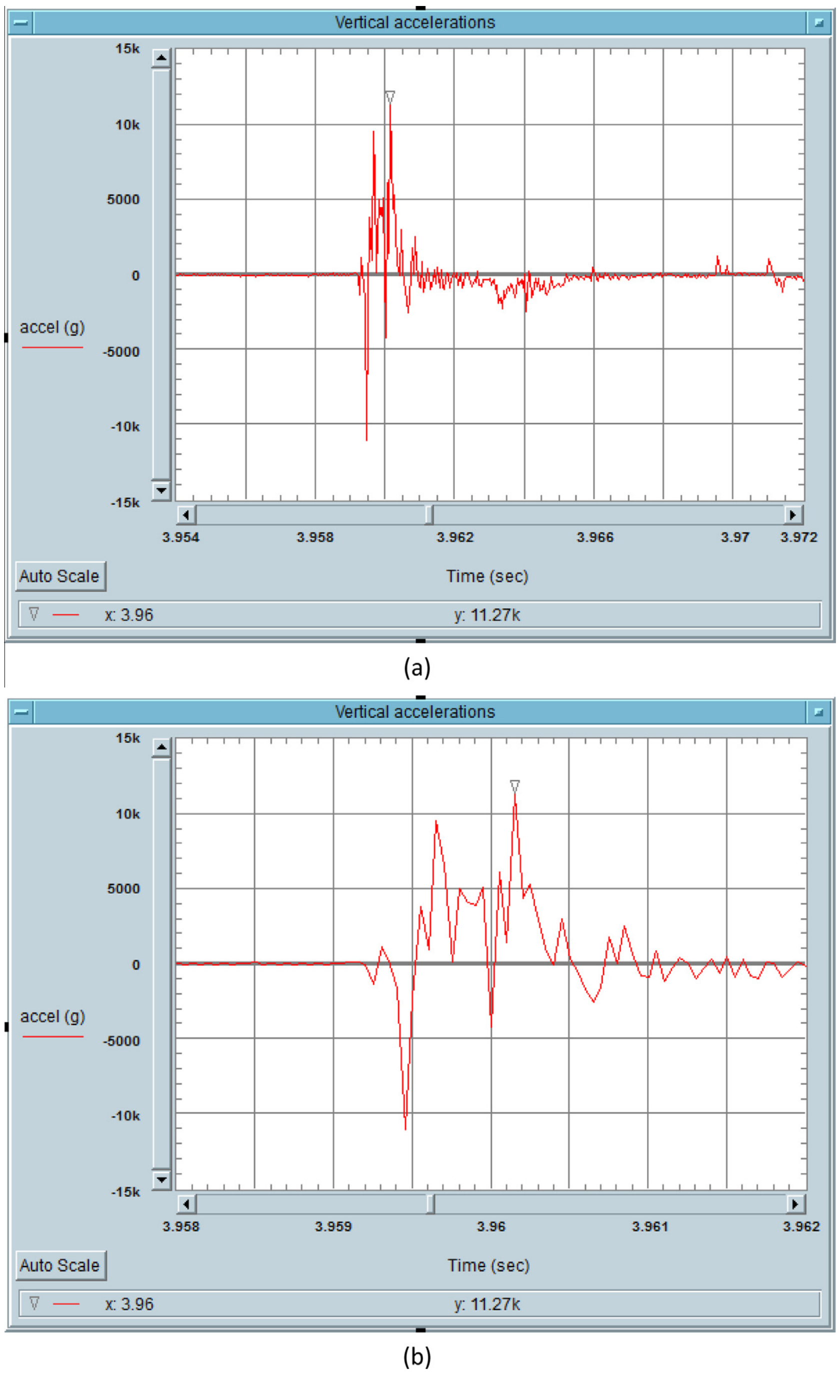

Fig. 9. Time history of the vertical accelerations measured on column 2. (a) Full record; (b) zoom.

Table 1
Air properties.

γ	ρ [kg/cm^3]	θ [K]	C_v [J/kg K]	e [kJ/m^3]
1.4	1.223E^6	288	717.6	2.068E^5

where ρ_p is the density of the porous material and α is called material "porosity". The P-alpha default properties used in this study are shown in Table 3.

The RHT strength model is a combined plasticity and shear damage model in which the deviatory stress Y = $\sqrt{3J_2}$ is limited by a generalized failure surface defined as

$$Y_{fail}(p^*, \theta, \dot{\varepsilon}) = Y_{TXC}(p^*)R_3(\theta)F_{Rate}(\dot{\varepsilon}) \quad (8)$$

$$Y_{TXC}(p^*) = f'_c[A(p^* - p^*_{spall}F_{Rate}(\dot{\varepsilon}))^N] \quad (9)$$

Table 2
TNT properties (EOS JWL).

ρ [g/cm^3]	A [kPa]	B [kPa]	R_1	R_2	ω	$V_{C\text{-}J}$ [m/s]	$e_{C\text{-}J}$ [kJ/m^3]	$p_{C\text{-}J}$ [kPa]
1.63	3.7377E^8	3.7471E^6	4.15	0.90	0.35	6.93E^3	6.0E^6	2.1E^7

Table 3
P-alpha default parameter setting.

B_0	B_1	A_1 [kPa]	A_2 [kPa]	A_3 [kPa]	T_1 [kPa]	T_2 [kPa]
1.22	1.22	3.527E^7	3.958E^7	9.04E^6	3.527E^7	0.0

where f'_c is the uniaxial compression strength; A and N are material constants; $p^* = p/f'_c$ is the normalized pressure, p is the hydrostatic pressure and $p^*_{spall} = f_t/f'_c$, where f_t is the uniaxial tension strength; $F_{Rate}(\dot{\varepsilon})$ represents the dynamic amplification factor (DIF) as a function of strain rate $\dot{\varepsilon}$.

$R_3(\theta)$ is a reduction factor of the surface Y_{fail}, that takes into account the dependence with the Lode angle θ, rotation about the hydrostatic axis. The ratio Q_2 of tensile to compressive meridian decreases with increasing pressure. This effect is called "brittle to ductile transition" and is described by

$$R_3(\theta, Q_2) = \frac{2\left(1-Q_2^2\right)\cos\theta + (2Q_2-1)\sqrt{4\left(1-Q_2^2\right)\cos^2\theta + 5Q_2^2 - 4Q_2}}{4\left(1-Q_2^2\right)\cos^2\theta + (1-2Q_2)^2} \tag{10}$$

$$0,5 < Q_2 = Q_{2.0} + B_Q p^* \leqslant 1 \tag{11}$$

$$\cos 3\theta = \frac{3\sqrt{3}J_3}{2(J_2)^{3/2}} \tag{12}$$

where $Q_{2.0}$ is tensile to compressive meridian ratio, B_Q is brittle to ductile transition defined by the rate at which the fracture surface changes from an approximately triangular form to a circular form with increasing pressure, J_2 and J_3 represent the second and the third invariants of the deviatory stress tensor.

Strain rate effects are represented through increases in fracture strength with plastic strain rate.

$$F_{Rate} = \begin{cases} 1 + \left(\frac{\dot{\varepsilon}}{\dot{\varepsilon}_0}\right)^{\alpha}, & \dot{\varepsilon}_0 = 30\mathrm{E}^{-6}s^{-1} \quad for \quad p \geqslant \frac{1}{3}f'_c \\ 1 + \left(\frac{\dot{\varepsilon}}{\dot{\varepsilon}_0}\right)^{\delta}, & \dot{\varepsilon}_0 = 3\mathrm{E}^{-6}s^{-1} \quad for \quad p < \frac{1}{3}f_t \end{cases} \tag{13}$$

where α is the compression strain rate factor and δ is the tension strain factor.

The elastic limit surface is scaled down from the fracture surface

$$Y_{elast} = Y_{fail}F_{elast}F_{cap} \tag{14}$$

$$F_{elast} = \begin{cases} \frac{f_{t,el}}{f_t}, & if \quad p < \frac{f_{t,el}}{3f_t} \\ \frac{f_{c,el}}{f'_c}, & if \quad p > \frac{f_{c,el}}{3f'_c} \end{cases} \tag{15}$$

F_{elast} is the ratio of the elastic strength to failure surface strength derived from two input parameters (elastic strength/f'_c) and (elastic strength/f_t).

A residual (frictional) failure surface is defined as

$$Y^*_{fric} = B(p^*)^M \tag{16}$$

where B is the residual failure surface constant and M is the residual failure surface exponent, both input parameters.

Damage is assumed to accumulate due to inelastic deviatory straining (shear induced cracking) using the relationships

$$D = \sum \frac{\Delta\varepsilon^{pl}_{eq}}{\varepsilon^{pl,fail}_{eq}(p^*)} \tag{17}$$

$$\varepsilon^{pl,fail}_{eq}(p^*) = D_1\left(p^* - p^*_{spall}\right)^{D_2} \geqslant e^{fail}_{\min} \tag{18}$$

where D_1 and D_2 are material constants used to describe the effect strain to fracture as a function of pressure.

Table 4
RHT strength model, default parameter setting.

G [kPa]	f'_c [kPa]	f_t/f'_c	f_s/f'_c	A	N
1.09E^7	3E^4	0.1	0.18	1.6	6.1E^{-1}
$Q_{2.0}$	B_Q	$\frac{G_{elast}}{G_{elast}-G_{plas}}$	$f_{t,el}/f_t$	$f_{c,el}/f'_c$	B
6.805E^{-1}	1.05E^{-2}	2	0.7	0.53	1.6
m		α			δ
6.1E^{-1}		3.2E^{-2}			3.6E^{-2}

Table 5
RHT damage model, default parameter setting.

D_1	D_2	$e^{fail}_{\min}$	G_{fail}/G
4E^{-2}	1	1E^{-2}	1.3E^{-1}

The relation between Y_{fail} and Y^*_{fric}, is given by

$$Y_{damaged} = Y_{fail} + D(Y_{fric} - Y_{fail}) \tag{19}$$

The crack softening is considered for the response after the tensile failure [26].

$$k = \frac{f_t^2}{2G_F} \tag{20}$$

where k is the stiffness softened, G_F is the fracture energy and f_t is the tensile strength.

The RHT default properties used in this study are shown in Tables 4 and 5.

Where G is shear modulus, f_s is shear strength and $\frac{G_{elast}}{G_{elast}-G_{plas}}$ is the hardening slope.

Where G_{fail}/G is the residual shear modulus fraction.

4.1.4. Steel

The reinforcement steel is modelled as isotropic, linear elastic and strain hardening. It is strain rate dependent with thermally softening plasticity. For hydrostatic pressure, steel compression is approximately proportional to pressure level. Thus, the elastic response is defined by a linear EOS. The pressure level is dependent on the bulk modulus K and the function of density μ for compression as

$$p = K\mu \tag{21}$$

$$\mu = \frac{\rho}{\rho_0} - 1 \tag{22}$$

The plastic response is defined by the Johnson and Cook [27] strain hardening, strain rate effective, and pressure softening material constitutive law. The yield strength Y is given by

$$Y = [\sigma_0 + B_s(\varepsilon^p)^{ns}][1 + C_s \log \dot{\varepsilon}^*_p][1 - T_H^{ms}] \tag{23}$$

where σ_0 the initial yield stress, ε^p is the plastic strain, $\dot{\varepsilon}^*_p$ is the plastic strain rate, B_s and ns represent the effect of strain hardening, C_s and ms are the material constants and T_H is the homologous temperature

$$T_H = \frac{T - T_{room}}{T_{melt} - T_{room}} \tag{24}$$

where T is the material temperature, T_{melt} is the melting temperature and T_{room} is the room temperature. The Steel default properties used in this study are shown in Tables 6 and 7.

Table 6
Steel properties (linear EOS).

ρ [g/cm^3]	K [kPa]	T_{room} [K]	S [J/kg K]	λ [J/mK s]
7.83	1.59E^8	3.0E^2	4.77E^2	0

Table 7
Steel properties (JC strength model).

G [kPa]	f_y [kPa]	B [kPa]	n	C	m	T_{melt} [K]
8.18E^7	4.2E^5	5.1E^5	2.6E^{-1}	1.4E^{-2}	1.03	1.793E^3

Where S is the specific heat, λ is the thermal conductivity, G is the shear modulus, f_y is the yield stress, C is the strain rate constant and m is the thermal softening.

4.2. Model description

A numerical model of 2.6 m $\times$ 0.4 m $\times$ 1 m was built in AUTODYN [21] reproducing the experimental test (Fig. 10). First, the explosion was modelled in a 2D axial symmetric model of 2 mm cells and then was remapped to a 3D model. An Euler FCT mesh was used for the air and a finite element mesh was used for the

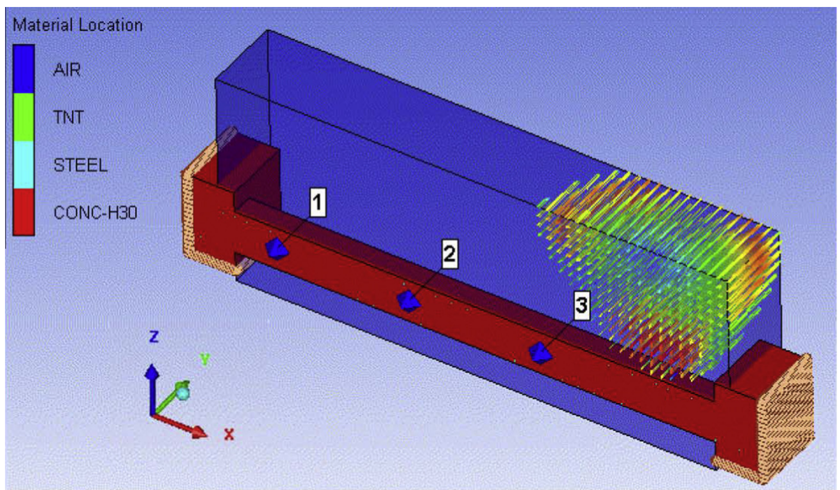

Fig. 10. Numerical model.

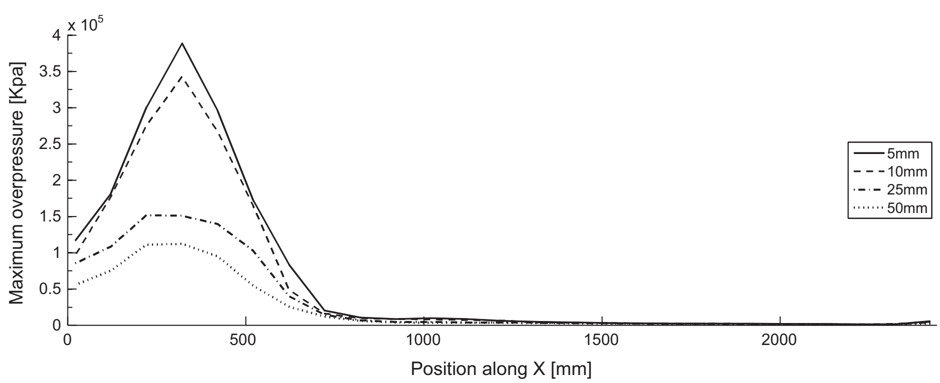

Fig. 11. Maximum overpressure registered in the front face of the RC member.

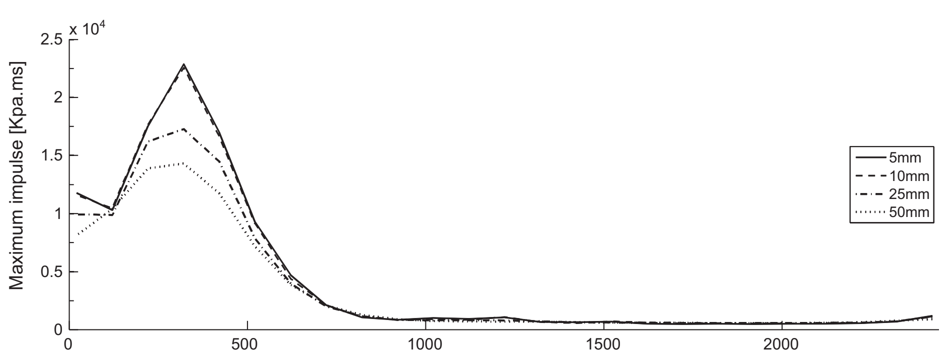

Fig. 12. Maximum impulses registered in the front face of the RC member.

concrete and the reinforcement steel bars were discretized into beam elements. The mesh size of the concrete, steel bars and the air was 10 mm. Given that in the experimental test the concrete blocks did not suffer any displacement or rotation, the blocks were partially modelled and velocity 0 was imposed at the ends of the blocks as boundary condition clamping the member. The symmetry of the problem also allowed modelling a half of the RC member. The boundary condition of the air was set as flow out boundary condition and the ground was rigid and allowed wave reflection.

4.3. Erosion

In order to simulate the physical damage of the concrete under the blast such as spalling and crushing, an erosion algorithm is

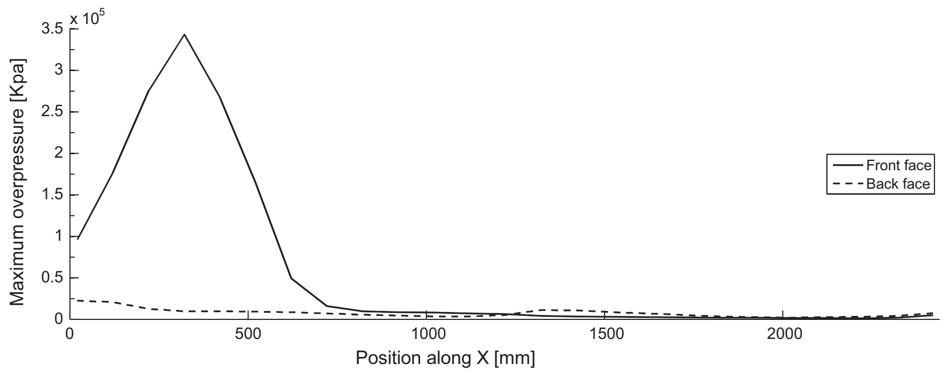

Fig. 13. Maximum overpressures recorded in the front and back face of the RC member.

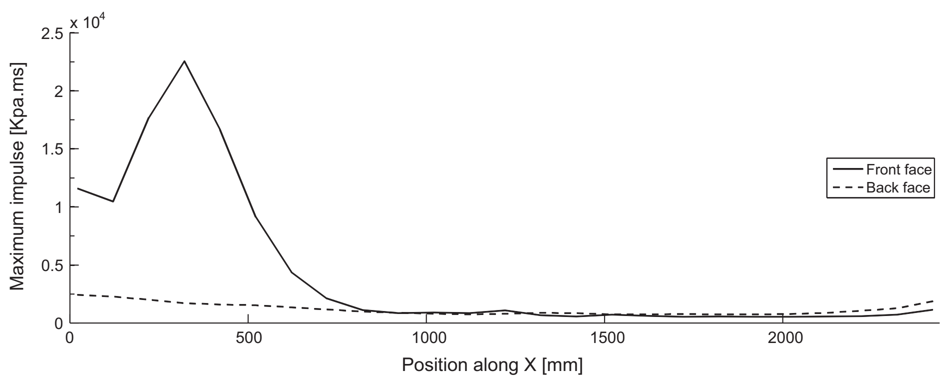

Fig. 14. Maximum impulses recorded in the front and back face of the RC member.

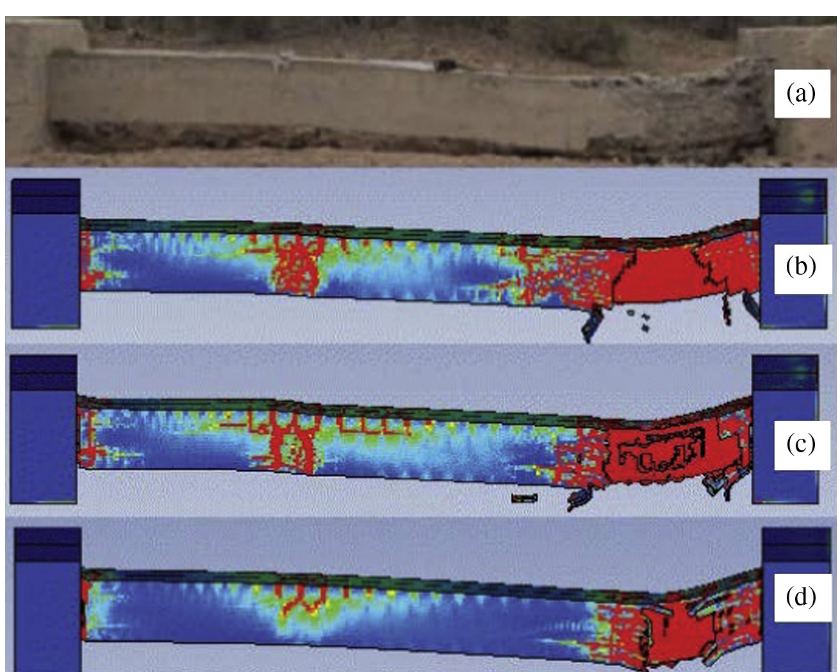

Fig. 15. Damage in column 2. (a) Experimental test. (b) Contours using default parameter setting. (c) Contours using Tu and Lu [15] parameter setting. (d) Contours using proposed parameter setting.

usually adopted. Erosion is initiated when an instantaneous geometric strain limit is reached given by the following equation:

$$\varepsilon_{inst} = \frac{2}{3}\sqrt{\left(\varepsilon_{11}^2+\varepsilon_{22}^2+\varepsilon_{33}^2\right)+5\left(\varepsilon_{11}\varepsilon_{22}+\varepsilon_{22}\varepsilon_{33}+\varepsilon_{33}\varepsilon_{11}\right)-3\left(\varepsilon_{12}^2+\varepsilon_{23}^2+\varepsilon_{31}^2\right)} \tag{25}$$

The instantaneous geometric strain can increase or decrease with loading and unloading but once an element has been eroded it can no longer be recovered. After many simulations, a value of 0.5 is adopted for concrete.

4.4. Mesh sensitivity

A study of the air mesh sensitivity was performed in order to validate the size element. Four models were built with element size for air of 5 mm, 10 mm, 25 mm and 50 mm. The maximum overpressure and impulse were obtained along gauge points in front face of the RC member. In Figs. 11 and 12, there is a 12% difference between the 5 and 10 mm models for the overpressures and another difference of lower than 2% for the impulses. Hence, a model with 10 mm elements is acceptable and decreases the computational time 10 times.

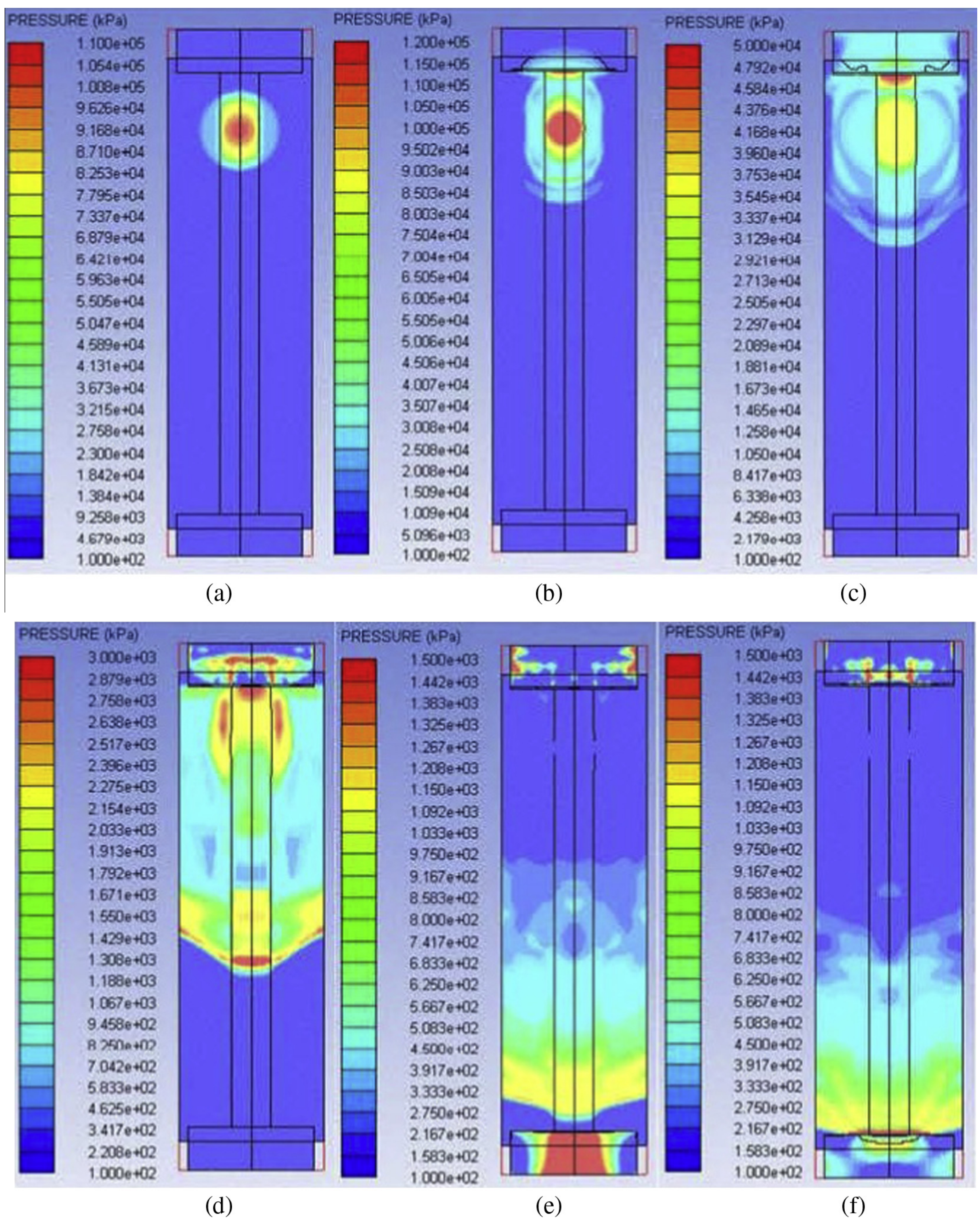

Fig. 16. Predicted pressure contour over the column 2. (a) Time 2.043E−2 ms. (b) Time 7.196E−2 ms. (c) Time 1.421E−1 ms. (d) Time 3.945E−1 ms. (e) Time 9.239E−1 ms. (f) Time 1.046 ms.

Table 8
Parameter setting of RHT model.

	AUTODYN [21]	Tu and Lu [15]	This work
RHT model			
B	1.6	0.7	0.35
M	0.61	0.8	0.55
RHT damage model			
D_1	0.04	0.015	0.08
D_2	1	1	1
$e_{\min}^{fail}$	0.01	8.00E^{-4}	0.03

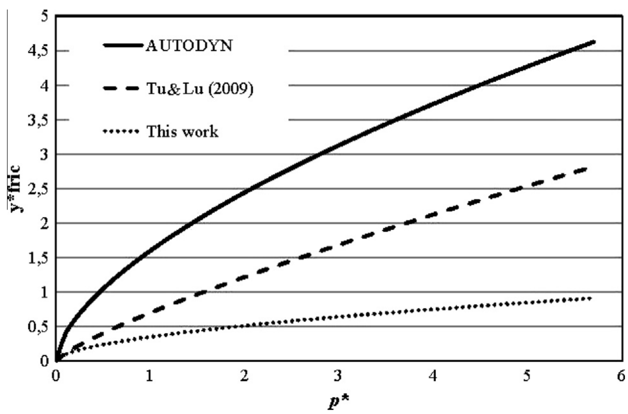

Fig. 17. Y^*_{fric} function for RHT model.

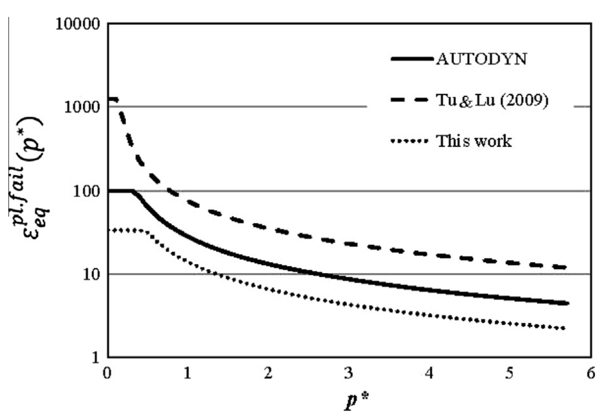

Fig. 18. $\left(\varepsilon_{eq}^{pl,fail}\right)^{-1}$ function for RHT model.

A mesh size of 10 mm for the concrete and steel bars was adopted in this study in consideration of the findings of Luccioni et al. [28] in which was demonstrated that a mesh of 10 mm has enough accuracy for similar problems.

4.5. Loading condition with ground interaction

It is clear that the loading condition on the specimen is very complex due to the interaction between shock wave, specimen and ground. Taking into account the final deformation of the member, it can be observed that shock wave reflection from the ground surface generates upward load acting on the specimen. This reflection is smaller than the direct blast load because counter-intuitive behaviour is not observed. However, this influence is negligible below the explosive as can be observed in Figs. 13 and 14.

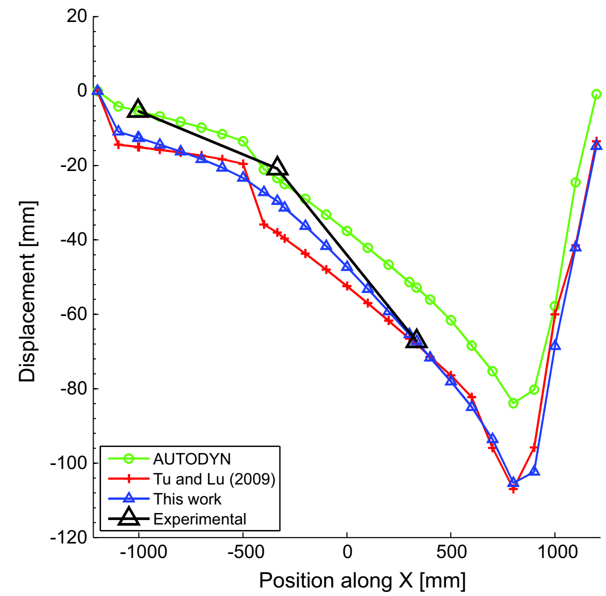

Fig. 19. Final vertical displacements of the column 2. $Z = 0.3$ m/kg$^{1/3}$.

4.6. Calibration of the numerical model

From the experimental test, the concrete member (column 2) was damaged in flexure mode (Fig. 15a) with concrete crushed on the front face, concrete spallation on the back surface and concrete flake off on the side surface. Also, it can be seen a second point of inflexion with deep cracks. First, the numerical model was carried out with the default parameters of RHT model available in AUTODYN and alternatively with parameters proposed by Tu and Lu [15]. The damage contours are presented in Fig. 15 (b) and (c) respectively. For both setups, the damage contours obtained were more pronounced than those observed in the real member. Besides, with the default values of AUTODYN the final displacement of the point near the explosion (point 3) was 21% lower than real one. In order to improve the model response, a new parameter setting was proposed based on the modification of the residual strength and the strength degradation. The results are presented in Fig. 15(d). It can be observed in the model that the crack patterns and the damage contour are improved with the new parameters and they resemble the ones observed in the experimental test.

On the other hand, the predicted pressure contour over the top face of the member is presented in Fig. 16. The reflection of the shock wave on both semi–buried concrete blocks can be seen at the end of the specimen.

The parameters used in the numerical model are shown in Table 8. The residual strength Y^*_{fric} was reduced by means of the parameter B and M (Eq. (16)). Also, the damage factor D_1, D_2 and $e_{\min}^{fail}$ (Eq. (18)) were modified to improve the strength degradation. The functions are presented in Figs. 17 and 18.

The vertical displacements of the column 2 are presented in Fig. 19. There is a 0.03% difference between the experimental test and the model with the parameter setting proposed in this work in the point near the explosion.

Fig. 20 shows that the erosion value of 0.5 can properly reproduce the concrete crushed on the front face, concrete spallation on the back surface and concrete flake off on the side surface observed experimentally. Besides, this value maintains the confined core of the column as observed in the experimental test.

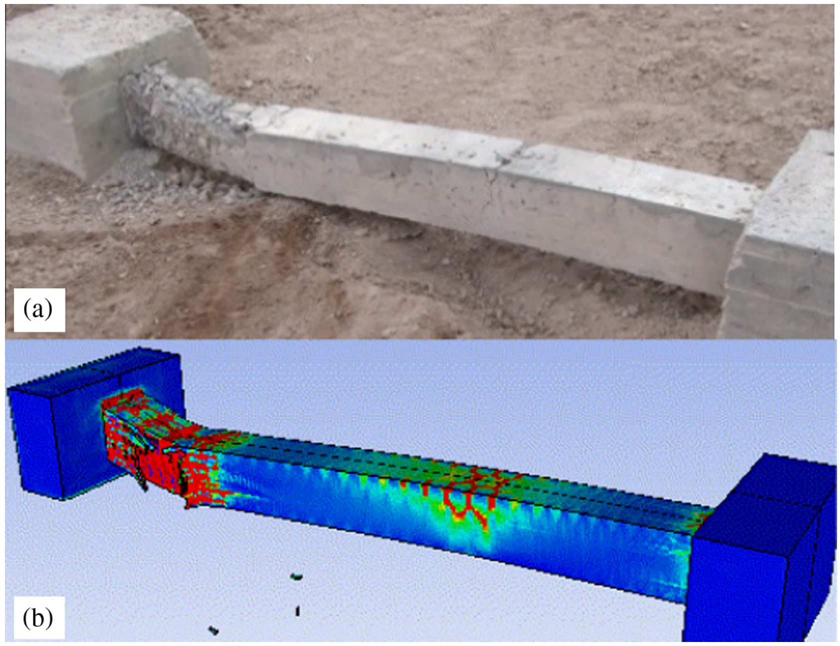

Fig. 20. Crack pattern and concrete spallation. (a) Experimental test. (b) Numerical model using proposed parameter setting.

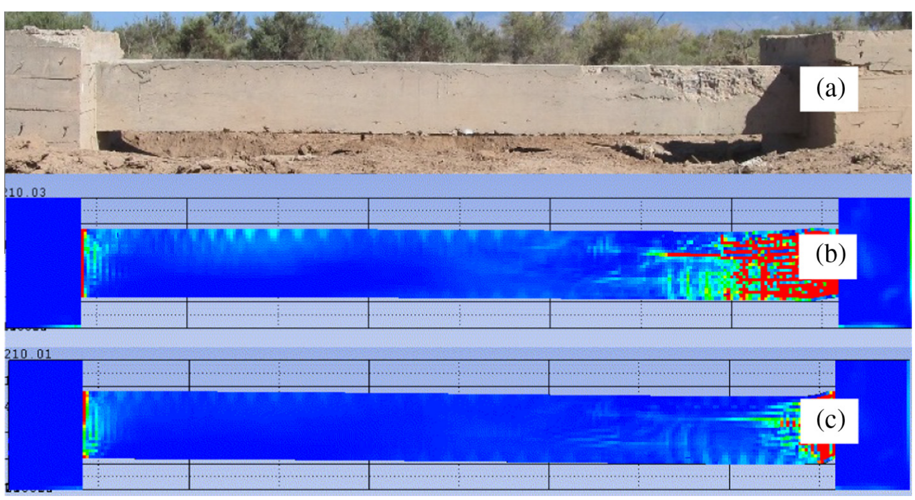

Fig. 21. Damage in column 1. (a) Experimental test. (b) Damage contours using default parameter setting. (c) Damage contours using proposed parameter setting.

4.7. Verification of the numerical model

The proposed parameters for the RHT model were also verified with the experimental results of column 1 subjected to 8 kg of TNT at 1 m. The damage results and the final displacements are presented in Figs. 21 and 22 respectively. The damage predicted by the default parameter setting can be seen that is more pronounced, but the final displacement is much lower than the actual member. The results obtained with the proposed parameter are in excellent agreement with the results observed in the experimental test.

4.8. Accelerations comparison

Finally, the time histories of the experimental and numerical accelerations for column 2, with $Z = 0.3\ \mathrm{m/kg^{1/3}}$ are presented in Fig. 23.

It should be noted that the accelerations obtained in the numerical model are much lower to those measured in the experimental test. The maximum acceleration value registered in the experimental test was 11,270 g while in the numerical model was 5631 g. It is evident that, although the numerical model is able to reproduce with enough accuracy the damage and final deflections of the RC members, it cannot faithfully reproduce the accelerations recorded.

On the other hand, considering that the accelerometer is located 120 cm from the center of the explosive, the shock wave generates an initial lifting of the area where the accelerometer is placed, which then is overcome by the deflection in the opposite direction. This inertial effect is also observed in the numerical study. The initial lifting occurs at an early stage of flexural strength for 0.0–3.6 ms. Then the column undergoes a phase transition to tension membrane resistance until reaching the maximum deflection [11].

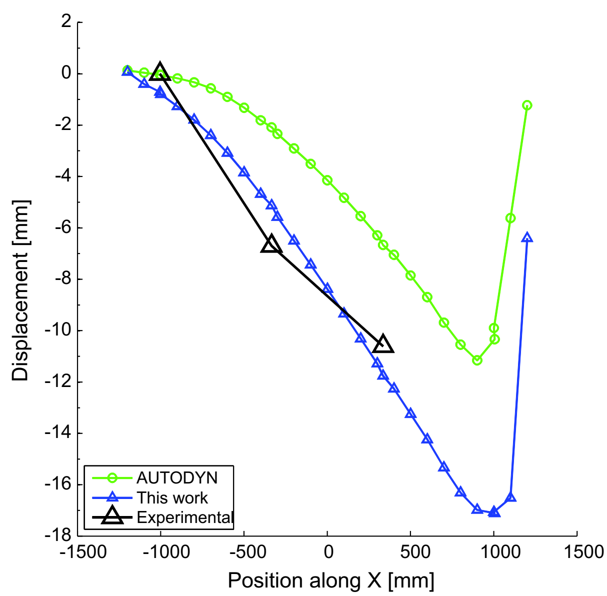

Fig. 22. Final vertical displacements of the column 1, $Z = 0.5$ m/kg$^{1/3}$.

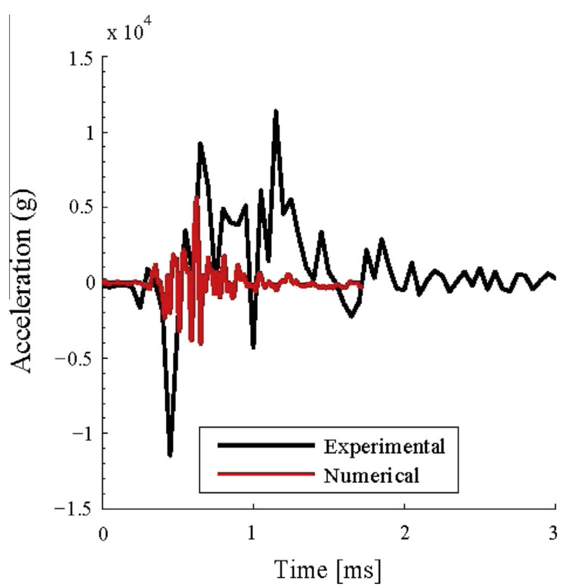

Fig. 23. Comparison of the experimental and numerical vertical accelerations on column 2.

5. Conclusions

Experimental tests of RC members subjected to a near field explosion were performed to study its dynamic response. Also, numerical models were carried out to calibrate the appropriate parameter setting of a RHT concrete model that allows for further predictions.

In this case, the default parameters of RHT model available in AUTODYN [21] and the alternative parameters proposed by Tu and Lu [15] show results with more pronounced damage contours than those observed in the actual members. The RHT modified model proposed in this paper is capable of reproducing not only the maximum displacement but also the general damage of the member and the crack pattern observed. However, the numerical model is not able to faithfully reproduce the accelerations recorded.

It should be noted that the proposed parameters are applicable to RC columns and very small scaled distances like those used in the experimental tests (0.5 and 0.3 m/kg$^{1/3}$). The default parameters of AUTODYN and those proposed by Tu and Lu [15] can be more useful for other situations.

Finally, it was showed that the erosion algorithm allows a good prediction of spallation effects. Also, a higher geometric strain limit than those found in other investigations is proposed for these very small scaled distances.

Acknowledgements

The cooperation in the blast tests of Prof. Oscar Curadelli, Bioeng. Gabriel Houri, Dr. Eng. Martín Domizio, Dr. Eng. Carlos Martínez and Dr. Eng Hernán Garrido are specially acknowledged. The financial support of CONICET (Argentina) and SECTYP (National University of Cuyo) is also gratefully acknowledged. Special acknowledgements are extended to the reviewers of the first version of the paper because their useful suggestions led to improvements of the work.

References

[1] Luccioni BM, Ambrosini RD, Danesi RF. Analysis of building collapse under blast loads. Eng Struct 2004;26(1):63–71.
[2] Abladey L, Braimah A. Near-field explosion effects on the behaviour of reinforced concrete columns: a numerical investigation. Int J Protect Struct 2014;5:475–500.
[3] Bao X, Li B. Residual strength of blast damaged reinforced concrete columns. Int J Impact Eng 2010;37:295–308.
[4] Parisi F. Blast fragility and performance-based pressure–impulse diagrams of European reinforced concrete columns. Eng Struct 2015;103:285–97.
[5] Dakhakhni W, Mekky W, Changiz S. Vulnerability screening and capacity assessment of reinforced concrete columns subjected to blast. J Perform Constr Facil 2009;23:353–65.
[6] Zhang D, Yao S, Lu F, Chen X, Lin G, Wang W, Lin Y. Experimental study on scaling of RC beams under close-in blast loading. Eng Fail Anal 2013;33:497–504.
[7] Fujikake K, Aemlaor P. Damage of reinforced concrete columns under demolition blasting. Eng Struct 2013;55:116–25.
[8] Ghani Razaqpur A, Tolba A, Contestabile E. Blast loading response of reinforced concrete panels reinforced with externally bonded GFRP laminates. Compos Part B Eng 2007;38:535–46.
[9] Pantelides C, Garfield T, Richins W, Larson T, Blakeley J. Reinforced concrete and fiber reinforced concrete panels subjected to blast detonations and post-blast static tests. Eng Struct 2014;76:24–33.
[10] Roller C, Mayrhofer C, Riedel W, Thoma K. Residual load capacity of exposed and hardened concrete columns under explosion loads. Eng Struct 2013;55:66–72.
[11] Astarlioglu S, Krauthammer T, Morency D, Tran T. Behavior of reinforced concrete columns under combined effects of axial and blast-induced transverse loads. Eng Struct 2013;55:26–34.
[12] Li J, Hao H. A simplified numerical method for blast induced structural response analysis. Int J Protect Struct 2014;5:323–48.
[13] Wang W, Zhang D, Lu F, Wang S, Tang F. Experimental study and numerical simulation of the damage mode of a square reinforced concrete slab under close-in explosion. Eng Fail Anal 2013;27:41–51.
[14] Li J, Wu C, Hao H. Residual loading capacity of ultra-high performance concrete columns after blast loads. Int J Protect Struct 2015;6(4):649–70.
[15] Tu Z, Lu Y. Evaluation of typical concrete material models used in hydrocodes for high dynamic response simulations. Int J Impact Eng 2009;2009(36):132–46.
[16] Yan B, Liu F, Song D, Jiang Z. Numerical study on damage mechanism of RC beams under close-in blast loading. Eng Fail Anal 2015;51:9–19.
[17] Li J, Wu C, Hao H. An experimental and numerical study of reinforced ultra high performance concrete slabs under blast loads. Mater Des 2015;82:64–76.
[18] Xu K, Lu Y. Numerical simulation study of spallation in reinforced concrete plates subjected to blast loading. Comput Struct 2006;84(5–6):431–8.
[19] Codina R, Ambrosini D, de Borbón F. Aternatives to prevent the failure of RC members under close-in blast loadings. Eng Fail Anal 2016;60:96–106.
[20] FEMA 426. Reference manual to mitigate potential terrorist attacks against buildings; 2003.
[21] ANSYS-AUTODYN. Interactive non-linear dynamic analysis software, version 16, user's manual. Century Dynamics Inc.; 2009.
[22] Remennikov A, Uy B. Simplified modeling of hollow and concrete – filled square tubular steel columns for near – field detonation. In: 15th International symposium on interaction of the effects of munitions with structures paper, 2013.

[23] Lee E, Tarver C. Phenomenological model of shock initiation in heterogeneous explosives. Phys Fluids 1980;23(12):2362–72.
[24] Riedel W, Thoma K, Hiermaier S, Schmolinske E. Penetration of reinforced concrete by BETA-B-500 - numerical analysis using a new macroscopic concrete model for hydrocodes. In: Proc 9, ISIEMS, Berlin, Strausberg, 1999; p. 315–22.
[25] Herrmann W. Constitutive equation for the dynamic compaction of ductile porous materials. J Appl Phys 1969;40(6):2490–9.
[26] Leppännen J. Concrete subjected to projectile and fragment impacts: modelling of crack softening and strain rate dependency in tension. Int J Impact Eng 2006;32:1828–41.
[27] Johnson G, Cook W. A constitutive model and data for metals subjected to large strains, high strain rates and high temperatures. In: Proc 7th int symp on ballistics, Hague, Netherlands, 1983; p. 541–7.
[28] Luccioni B, Araoz G, Labanda N. Defining erosion limit for concrete. Int J Protect Struct 2013;4(3):315–40.